scientific reports

Check for updates

OPEN

Multi-gas dual-comb spectroscopy with tunable gain-switched laser diodes

L. Monroy[1,2]✉, A. Pérez-Serrano[1], J. M. G. Tijero[1]✉ & I. Esquivias[1]

This study presents a tunable multi-gas spectroscopic scheme using a dual-comb architecture operating within the near-infrared domain. The dual-comb signal is generated by two gain-switched Fabry–Perot laser diodes at low repetition rates and externally injected by a tunable laser source. A systematic study on the injection wavelength, line spacing and optical span performed over the system, ensures the generation of stable optical frequency combs with a 40 GHz bandwidth, and more than 400 lines at a low repetition rate (100 MHz). This system covers a wavelength range exceeding 40 nm, thereby enabling the characterization of different gases with molecular absorptions within this range. A proof-of-concept demonstration was conducted by analyzing four different gas samples, showing similar results to those provided by HITRAN and the manufacturer with a standard deviation of the residuals of 0.005. The simplicity and tunability of this configuration make it highly replicable, paving the way for commercial applications.

In recent decades, optical frequency combs (OFCs) have emerged as a cornerstone in cutting-edge applications, such as gas spectroscopy[1], optical communications[2], optical atomic clocks[3], and distance metrology[4,5], among others. These short- duration coherent pulses are constituted by an array of discrete, equally spaced narrow spectral lines (tones). Multiple techniques have been employed for comb generation using semiconductor lasers. Among them, mode-locked lasers[6] and microcombs[7] demonstrate large bandwidths and high optical powers. However, such methods are often hampered by complex and costly manufacturing processes and have a fixed repetition rate determined by the cavity length. Although OFCs generated by electrooptic (EO) modulation[8] and gain-switching (GS)[9] techniques applied to semiconductor lasers exhibit narrower bandwidths, they feature variable repetition rates that can be adjusted from tens of GHz down to tens of MHz, because they are determined by the signal modulation frequency rather than the cavity length. Among these, gain-switched lasers have garnered interest for their simplicity, compactness, and ease of implementation[10,11].

The GS technique involves the modulation of a semiconductor laser through the application of a tunable repetition rate periodic radio-frequency (RF) voltage (AC signal), superimposed on a bias current (DC signal). Typically, sinusoidal signals are used for AC modulation when operating at repetition rates between 5–25 GHz, resulting in the generation of broad and flat OFCs with well-defined tones[10,12]. However, at lower repetition rates (< 500 MHz), the coherence between consecutive pulses may be compromised as they arise from spontaneous emission of the GS laser[13,14]. This effect can be avoided through pulsed electrical excitation and optical injection locking (OI)[15–17]. Furthermore, OI enhances comb coherence by transferring the linewidth of the external laser to each individual comb line[9]. This facilitates the generation of high-quality OFCs, characterized by improved spectral flatness and an increased number of comb lines. An example of this is the use of pulse-pattern generators as the RF source, resulting in flat and broad combs at 5 MHz repetition rate, with a spectral width of 133 GHz, encompassing 1200 tones at 10 dB[18]. However, the reliance on such high data-rate driving sources has proven to be both costly and cumbersome. For cost-effective GS-OFC generation, there is a growing demand for low-cost electronics capable of producing high-quality optical signals without compromising accuracy, robustness, and resolution. In this context, the use of low-cost step-recovery diodes (SRDs) to generate broad and stable OFCs has been explored[19], along with the integration of a software-defined radio as a low-cost detection unit[20]. These combs have been shown to be suitable for gas sensing applications using the dual comb spectroscopy (DCS) technique. They can be employed for applications requiring low line spacing, and broad bandwidths, such as in gas spectroscopy.

In recent years, DCS has emerged as a highly promising technique, showing superior performance, resolution, and sensitivity[21]. Compared to conventional techniques, DCS offers significant advantages in precision and fast

[1]CEMDATIC - E.T.S.I. Telecomunicación, Universidad Politécnica de Madrid, 28040 Madrid, Spain. [2]Electronics Technology Department, Universidad Carlos III de Madrid, C/Butarque 15, 28911 Leganés, Madrid, Spain. ✉email: lmonroy@ing.uc3m.es; jm.g.tijero@upm.es

acquisition times, owing to its compact and scanless characteristics[22–24]. DCS entails the use of two OFCs with slightly different repetition rates f_1 and f_2, whose beating on a photodetector results in an RF comb spectrum with tones separated by a frequency $\Delta f_R = f_2 - f_1$. The spectroscopic data of the gas under study are encoded within the optical spectra of the OFCs and are subsequently transferred to the down-converted RF comb replica. Thus, one comb is effectively "sampled" by the other, eliminating the requirement for dispersive elements or mobile components.

Previous studies have demonstrated the development of high-quality dual-comb spectrometers by using these gain-switched combs. An example of this was the generation of flat-topped, low repetition rate dual frequency combs in the near-infrared (NIR) region for the measurement of the absorption profiles of hydrogen cyanide (HCN) and carbon dioxide (CO_2)[20,25,26]. In these experiments, the application of pulsed electrical signals as the excitation source of two commercial distributed feedback (DFB) lasers, combined with external optical injection, resulted in a spectral resolution as low as 100 MHz. This resolution can be further enhanced by reducing the repetition rate of the excitation signal. This can be performed by densifying the comb lines using an external electro-optic phase modulator (EOPM). An increase of up to 12000 lines separated by a 3.93 MHz repetition rate has been reported recently[27,28], with a 25-fold improvement in resolution. However, this system still entails high complexity and cost for spectroscopic applications and offers limited tunability in the spectral range due to the use of a monomode laser.

Several strategies have been explored in order to overcome the spectral bandwidth limitation and extend the spectral range attainable with the OFCs generated by GS. Spectral broadening by using highly non-linear fibers has been reported in edge emitting GS lasers[11] as well as in VCSELs[29]. The use of two independent GS lasers and a phase modulator, together with a SOA to induce the required phase coherence has also been reported[30], as well as the common injection of two OFCs in the spectral region where they overlap[31]. Fabry-Perot (FP) lasers have also been used for broadening purposes, either by cascading two GS FP lasers and optically injecting one of the longitudinal modes of one of them[32], or by optically injecting two or more adjacent modes of a single GS FP laser[33,34]. Instead of expanding the spectral width of an OFC, another approach consists in increasing the tunability of the OFC generator by tunable optical injection (one at a time) of multiple longitudinal modes within the gain region of a single FP laser under GS[35,36]. This approach is particularly suitable for spectroscopic applications, such as DCS of gases whose narrow spectral footprints are spread over relatively broad spectral regions, thus requiring dense and spectrally agile OFCs that span only the specific narrow wavelength region where the footprint of a particular gas lies, rather than a dense, broad, and highly coherent single OFC that spans the entire spectral range. This approach has been used in DCS[37] to measure the absorption profile of a single gas, hydrogen sulfide around 1574.5 nm.

Based on this approach, in this work we present a dual comb spectrometer capable of measuring with high resolution the spectral footprints of several gases in the NIR region around 1550 nm. Our system integrates a custom-built pulsed excitation source, using a direct digital synthesizer (DDS) and SRDs as the electrical signal generator. The main advantage of our system is the capability to cover a wide spectral range by optically injecting at different FP laser longitudinal modes with a tunable laser, thus allowing the measurement of different gases that show absorption in a C-band spectral range of 40 nm. To validate the capability of this DCS platform for gas monitoring, we conduct absorption measurements of various gas samples, including NH_3, HCN, CO and CO_2 in closed gas cells. This demonstration shows the versatility of our tunable DCS system for high-resolution measurements across both the C and L band regions with a single setup.

Experimental technique

Setup

The experimental setup, as illustrated in Fig. 1, is based on a dual-comb architecture, with two gain-switching OFCs operating at low repetition rates in the near-infrared region. The optical sources comprise two low-cost Fabry-Perot lasers centered at 1550 nm, without a built-in optical isolator to facilitate OI. To generate the

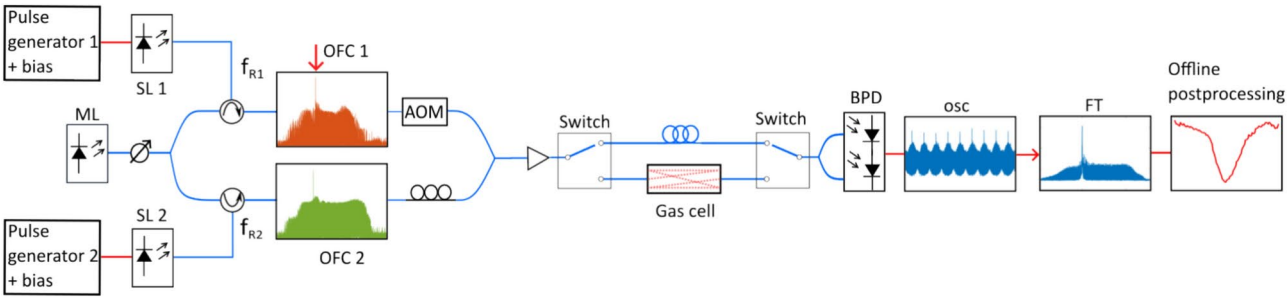

Fig. 1. Diagram of the dual-comb spectroscopy setup based on the combination of two OFCs, generated by optically injected FP-GS lasers in a master–slave laser configuration. The transmission of the OFCs through the gas cell is controlled by an optical switch, and their beating signal in a balanced photodiode is recorded by a high-bandwidth oscilloscope. Components: SL (Slave Laser), ML (Master Laser), AOM (Acousto-Optic Modulator), PC (Polarization Controller), BPD (Balanced Photodiode), OSC (Oscilloscope). Red lines represent electrical wires, whereas blue lines are optical connections.

corresponding OFCs, the gain-switching technique is applied by biasing the lasers with a DC current and an AC pulse train. A complete description of this process is explained in the Methods section.

Once the FP lasers are gain-switched, the phases of both lasers can be locked by inserting an optical injection source in a master-slave configuration, thus preserving the coherence of the generated pulse train[15]. In this configuration, the light from a tunable laser (TL), acting as a master laser (ML), is injected into each GS slave laser (SL) via two optical circulators, providing mutual coherence between the two combs[9]. The panels in Fig. 1 show the optical spectra of both OFCs (OFC1 and OFC2) measured with a high-resolution Brillouin optical spectrum analyzer (BOSA) (Aragon Photonics 210). Both combs show high density of lines and flatness.

In this case, the repetition rates are 100 MHz (f_{R1}) and 100.01 MHz (f_{R2}) for OFC1 and OFC2, respectively. The two OFCs are combined by using a 3 dB optical coupler, and their beating signal in a balanced photodiode is maximized by means of a polarization controller. An acousto-optic modulator (AOM, AA Opto-Electronic MT80-IIR30-Fio-PM0) is also incorporated, introducing a slight frequency shift between the combs (80 MHz), thus ensuring unambiguous identification of the beat frequencies, and mitigating the effects of flicker noise[38], Furthermore, to ensure the alignment between the master and slave lasers, the fibers before the AOM are polarization maintaining (PM). The gas absorption is then acquired by transmitting the optical combs through the gas sample in transmission configuration. To improve the signal-to-noise ratio (SNR) a symmetrical configuration is adopted. Two optical switches are used to perform two consecutive measurements, directing the optical combs either to a reference arm or to the gas cell. In this work, four different closed gas cells (Wavelength References Inc.) are measured. These cells contain NH_3, HCN, CO and CO_2 respectively. To maximize the gas absorbance, the length of each gas cell and the pressure is tailored as it is detailed later.

After passing through the gas under test, the two combs are detected by a 100 MHz balanced photodetector (BPD) (Koheron PD100B). The beating of the two OFCs in the photodetector generates an interferogram that is scrutinized using an oscilloscope (Keysight, MSOS804A). In the spectral domain, this corresponds to a radio frequency (RF) comb with a spacing of Δf_R. Consequently, the optical spectrum undergoes down-conversion by a compression factor (CF) of $f_R/\Delta f_R$. The spectral characteristics of the absorption of the gas under test, which are embedded in the optical spectra of the OFCs upon interaction with the sample, are also imprinted in the RF comb. Subsequently, a post-processing procedure is applied to discern the absorption line from the RF spectra by comparing the reference trace with the one conveying gas absorption information. Further discussion on this process is provided in the Methods section.

Spectral characterization of the Fabry-Pérot laser

In this section, the spectral profile of the FP laser under gain-switching operation is studied with and without optical injection. An example of the CW emission spectrum of a FP laser with a threshold current of 11 mA is shown in Fig. 2a, as measured with an optical spectrum analyzer (OSA) (Ando, AQ-6315B) with a resolution of 6 GHz. When operated at 25 °C and 30 mA, the peak emission of the FP laser is centered at 1547 nm and the FP modes cover almost 100 nm. The free spectral range (FSR) is 120 GHz (~ 1 nm), as depicted in the zoomed portion of Fig. 2a.

For gain-switching operation, the FP laser is biased with a DC current of 5.6 mA, and a pulsed AC signal with 7 V peak-to-peak and a repetition rate of 100 MHz generated by an RF source (see more information in the Methods section). Figure 2b shows the spectrum under gain-switching operation of the FP laser, with the corresponding broadening for each longitudinal mode. Owing to the absence of mode selectivity, the optical output contains all longitudinal modes of the FP laser. This results in a multimode spectrum, where each

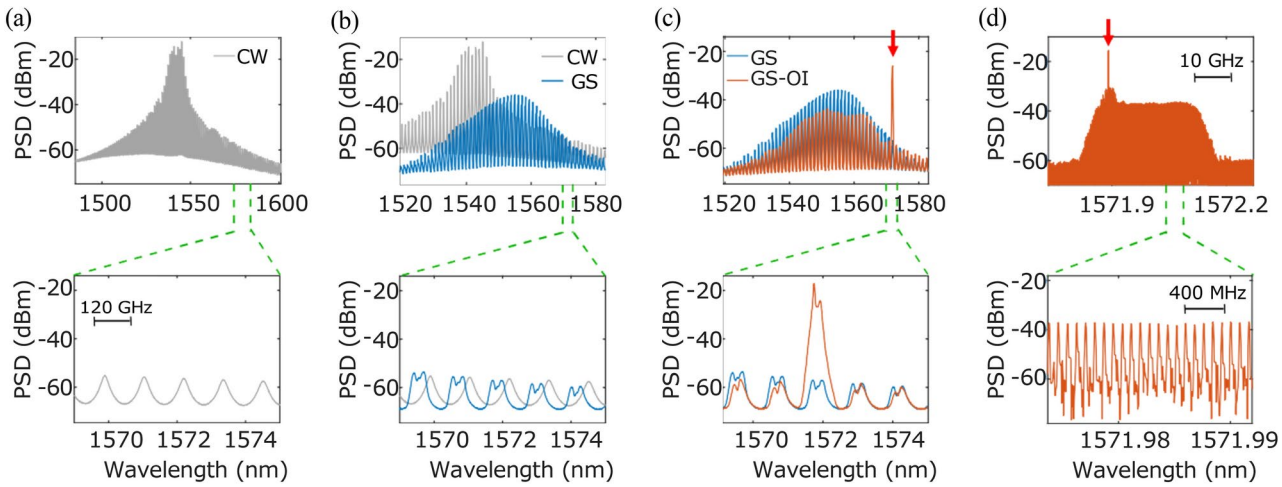

Fig. 2. Spectral characterization of the FP laser: (**a**) In continuous-wave (CW) operation at 25 °C and with a bias current of 30 mA. (**b**) By gain-switching the FP laser with an AC signal at 100 MHz and 7 V of amplitude (blue line) and with a bias current of 5.6 mA. (**c**) Applying optical injection at 1572 nm (orange arrow) with a power of -3.5 dBm locking the GS-FP laser. (**d**) Zoomed portion of the externally locked GS OFC registered by a BOSA.

longitudinal mode experiences spectral broadening compared to the CW spectrum due to the gain-switching mechanism. This yields to a change in the spectral profile of the FP laser due to the increased number of modes involved in the switch-on and switch-off dynamics of the laser. A redshift of the spectral envelope is also observed with respect to the CW operation, which can be attributed to the multimode gain dynamics in GS conditions. The zoomed portion of Fig. 2b highlights the gain-switching operation of the FP laser for the modes far from the central peak. To lock the optical phases and consequently enhance the coherence of the OFCs, an injection source is incorporated into the laser setup employing a master-slave configuration. Depending on the spectral region of interest, the injection wavelength of the ML is tuned to coincide with one of the longitudinal modes of the FP laser. This procedure can be applied to each longitudinal mode of the SL laser, thus increasing the spectral coverage with a single system. In this case, the laser could be locked from 1520 to 1600 nm.

The spectrum of the gain-switched FP laser with the injection peak of the ML centered at 1571.9 nm and marked with a red arrow is shown in Fig. 2c. It must be noted that injection locking is still feasible despite being far from the highest peaks of the spectrum of the gain-switched FP laser. The mode-selectivity obtained through optical injection results in single-mode performance with a side mode suppression ratio (SMSR) of 20 dB. Consequently, highly coherent OFCs can be generated by applying OI to a gain-switched FP mode under these operating conditions. The difference between the longitudinal mode profiles with and without the external injection can be observed in the zoomed portion of Fig. 2c. It is worth noting that due to the 6 GHz spectral resolution of the OSA, the individual tones of the optically injected GS-OFC cannot be resolved. Hence, only the envelope of the spectrum appears in these measurements. A closer examination of the OFC at 1572 nm, measured with the BOSA, is presented in Fig. 2d, demonstrating the spectral comb flatness with over 350 tones. The bandwidth of the externally injected GS-OFC, defined as the width at 10 dB (δf_{10}) is 35 GHz. Furthermore, a carrier-to-noise ratio (CNR) of 20 dB is attained, defined as the average value of the ratio between the intensities of those tones within δf_{10} and the noise level at frequencies between adjacent tones.

Results and discussion

Generation of tunable GS-OFCs

The tunability of the ML allows the generation of as many OFCs as the number of longitudinal modes of the FP laser and, together with temperature control, facilitate continuous wavelength tuning, thereby locking within a spectral range of 40 nm. Therefore, the absorption lines of the gas under study in this spectral range can be measured. The production of flat-topped OFCs was accomplished through a meticulous optimization process (see more details in the Methods section). The gain switching conditions (DC bias current, and RF modulation amplitude) and the OI conditions (injection power and wavelength) were optimized separately for each of the FP modes of interest. In addition, finer wavelength tunability was achieved by adjusting the temperature of the slave laser with a temperature controller. By detuning the injection wavelength to the edge of the FP mode, flat and wide OFCs were achieved, allowing the gas absorption lines contained within the combs to be measured. In our experiment, to prevent the instabilities arising close to the injection wavelength, it was detuned about 20 GHz from the absorption line of interest.

Figure 3 shows the optimized spectra of the appropriate OFCs for the absorption measurements of each gas in this study. The spectra were measured with the OSA (top panels) and the BOSA (bottom panels). They are centered on the position of the relevant absorption line of each gas, indicated by arrows in the bottom panels. Specifically, 1531.67 nm for the NH_3 (green line), 1549.73 nm for the HCN (blue line), 1569.45 nm for the CO

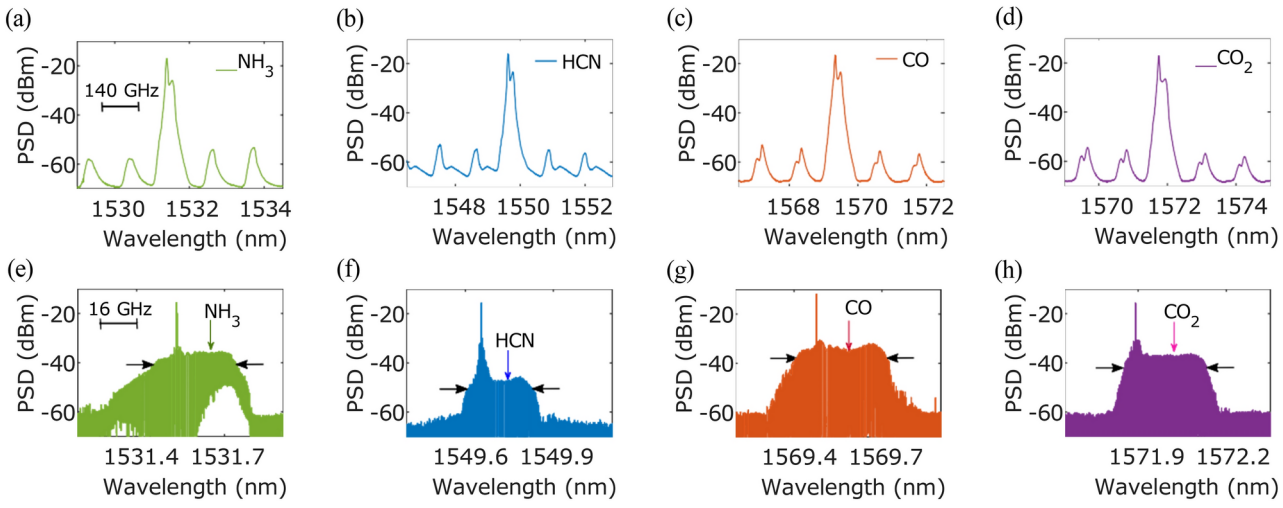

Fig. 3. Optical spectra measured with the OSA (top row) and the BOSA (bottom row) of the OFCs selected for measuring specific absorption lines of each gas in this study: NH_3, HCN, CO and CO_2, respectively. They are centered on the position of the corresponding absorption line of each gas (see text), indicated by arrows in the bottom panels. The prominent narrow peaks of the spectra are footprints of the optical injection. Horizontal arrows indicate δf_{10}.

Parameter	NH_3 (@ 1531.67 nm)	HCN (@ 1549.73 nm)	CO (@ 1569.45 nm)	CO_2 (@ 1572.02 nm)
δf_{10} (GHz)	35	29	37	36
CNR (dB)	25	17	26.5	24
Nº tones	345	290	375	357
SF	0.96	0.94	0.97	0.98

Table 1. Characteristics of the OFCs selected for measuring the absorption lines of each gas at the wavelength specified under the name of the gas in the first row.

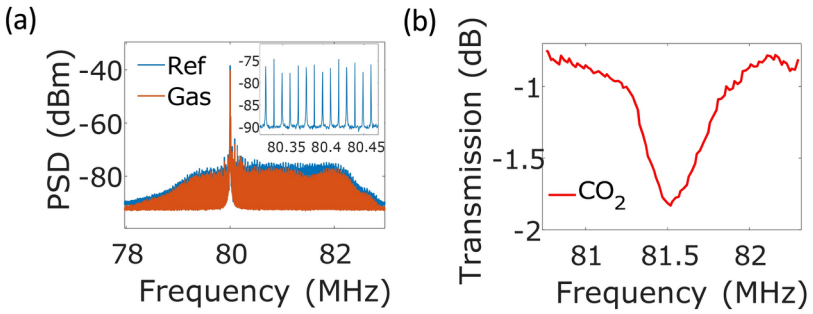

Fig. 4. (**a**) Down-converted RF spectrum of the reference measurement (blue line) and the one containing the gas cell (orange line). The inset shows a zoom portion of the reference RF trace where we can distinguish the different tones. (**b**) Transmission profile of the gas sample derived by substracting the RF spectrum of each comb.

(orange line) and 1572.02 nm for the CO2 (violet line). The prominent narrow peaks of the spectra in the bottom row are the footprint of the optical injection. From this figure, the difference in the spectral profiles of the four OFCs is noticeable. The OFC spectra generated from the FP longitudinal modes close to the maximum of the gain profile have lower powers and narrower bandwidths (see in particular the OFC centered at 1549.7 nm). Some instabilities are also observed for the OFC generated at 1531.5 nm. This is probably due to the location of the locked longitudinal mode, which is at the edge of the FP spectrum under gain-switching operation. In contrast, the OFCs generated around 1570 nm demonstrate superior performance due to the higher SMSR of the corresponding FP longitudinal mode. These differences will be further studied in future works.

To assess the quality of the optimized OFCs their spectra were characterized in terms of the spectral width (δf_{10}), the CNR, the number of tones, and the spectral flatness (SF). Under optimized conditions, an average spectral width of 35 GHz and with 350 clearly resolved comb tones are obtained for the four OFCs. A value of more than 17 dB is also obtained for the CNR of each OFC. Note that the peak resulting from the OI is excluded from CNR and δf_{10} calculations. Finally, the spectral flatness of the OFC, defined as the ratio of the geometric mean to the arithmetic mean of the power spectrum (maximum value, 1) has an average value of 0.96. Overall, these properties, together with their stability, make these OFCs suitable for gas absorption measurements. A summary of the characteristics of the OFCs selected for each absorption region is presented in Table 1.

Dual-comb spectroscopy

Finally, to assess the capability of the dual-comb system for high-resolution spectroscopy, absorption measurements of each gas were performed using the corresponding OFC. The gas absorption is derived by comparing the dual-comb spectra recorded when the optical switch routes the combs through the reference arm, and through the gas cell. The procedure for obtaining the absorption profile is described in the following paragraph with the help of Fig. 4, corresponding to the case of CO_2.

The temporal interferograms generated by the beating of the two OFCs are measured using the BPD. The RF electrical signal generated in the photodetector is then digitized using an oscilloscope. By applying the Fourier Transform (FT) to the temporal data, a down-converted RF comb is derived. Figure 4a illustrates the details of this comb. It shows that by using the dual-comb scheme, the width of the optical spectrum (see Fig. 3h) is compressed into a much narrower spectral window by a specific compression factor. The CF is determined by the repetition rate of each OFC and the difference between these values. In our experiment, the repetition rates are set to 100 MHz and 100.01 MHz, thus $CF = f_R/\Delta f_R = 10000$. To increase the SNR (signal-to-noise ratio) and enhance the resolution, 500 individual interferogram traces are recorded on the oscilloscope in 1 second and then averaged in frequency domain. The inset in Fig. 4a shows a magnified region of the RF spectrum of the reference trace. Clearly resolved comb tones with a CNR of 15 dB are apparent. The frequency spacing between them ($\Delta f_R = 10$ kHz) is also clearly seen. Figure 4a also shows that the spectral flatness is preserved for both the reference trace and the one containing the gas information which is an indication of the superior stability and phase-locking properties of our optically-injected GS-OFCs. After obtaining the RF combs corresponding to the reference and sample traces, the transmission spectrum is subsequently derived by subtracting both spectra

in logarithmic scale. A typical transmission profile is shown in Fig. 4b. The experimental gas absorption is then obtained after applying a linear baseline correction to the transmission curve. More details about the entire process are provided in the Methods section.

The absorption profiles measured for each gas sample are shown in Fig. 5. The NH_3 was enclosed in a 5.5 cm long gas cell at a pressure of 100 Torr. Its R4 line at 1531.67 nm was measured using 205 tones of the corresponding OFC. The gas cell containing HCN was 16.5 cm long and its pressure was also 100 Torr. Its R17 line at 1549.73 nm was measured using 135 tones of the corresponding OFC. The CO and CO_2 cells were both 80 cm long and their pressure was 500 Torr. Their R6 and R16 lines at 1569.45 and 1572.02 nm were measured using 170 and 165 tones of the corresponding OFCs, respectively. The absorption profiles were characterized in terms of Full-Width at Half-Maximum (FWHM) and transmittance (T) at the absorption peak. To do this, the experimental profiles were fitted to a Voigt functions shown by the red dashed lines in Fig. 5. The residuals of these fits are plotted in the bottom rows of each panel with a value as low as 0.005 (equivalent to a 0.3%). Also plotted in Fig. 5 are the profiles obtained using the parameters given in the HITRAN database[39] (green dashed lines) and in the manufacturer datasheet (orange lines). To help visualize the spectral width of the profiles, an upper x-axis in GHz units is added to each panel. For clarity, the frequency values on this axis are conveniently shifted so that the frequency of the absorption peak coincides with zero.

In Table 2 the experimental values of the width and transmittance and those resulting from the Voigt fit are compared with the values provided by the manufacturer and the HITRAN database. The experimental results align well with both data. Nevertheless, some differences are also noticeable. In the case of NH_3, two absorption lines have been measured within a spectral region of 20 GHz, centered at 1531.67 nm and 1531.73 nm, respectively. This demonstrates the capability of the system to discriminate between two nearby absorption lines (in this case with a separation as low as 0.08 nm) with enough resolution. Thus, a two-line Voigt fit has been applied in the postprocessing stage for this specific case. However, only the measurements of the spectral bandwidth and transmittance of the absorption line at 1531.67 nm are considered for comparison purposes. In the vicinity of this wavelength, the experimental absorption profile and the spectral profile in the manufacturer datasheet consist of a single line while the profile inferred from the HITRAN database points to a partially resolved double line. Since the resolution of our system is high enough to account for a double line profile, we do not know at present the reason for this discrepancy, which is also the origin of the difference between the experimental and the HITRAN bandwidth.

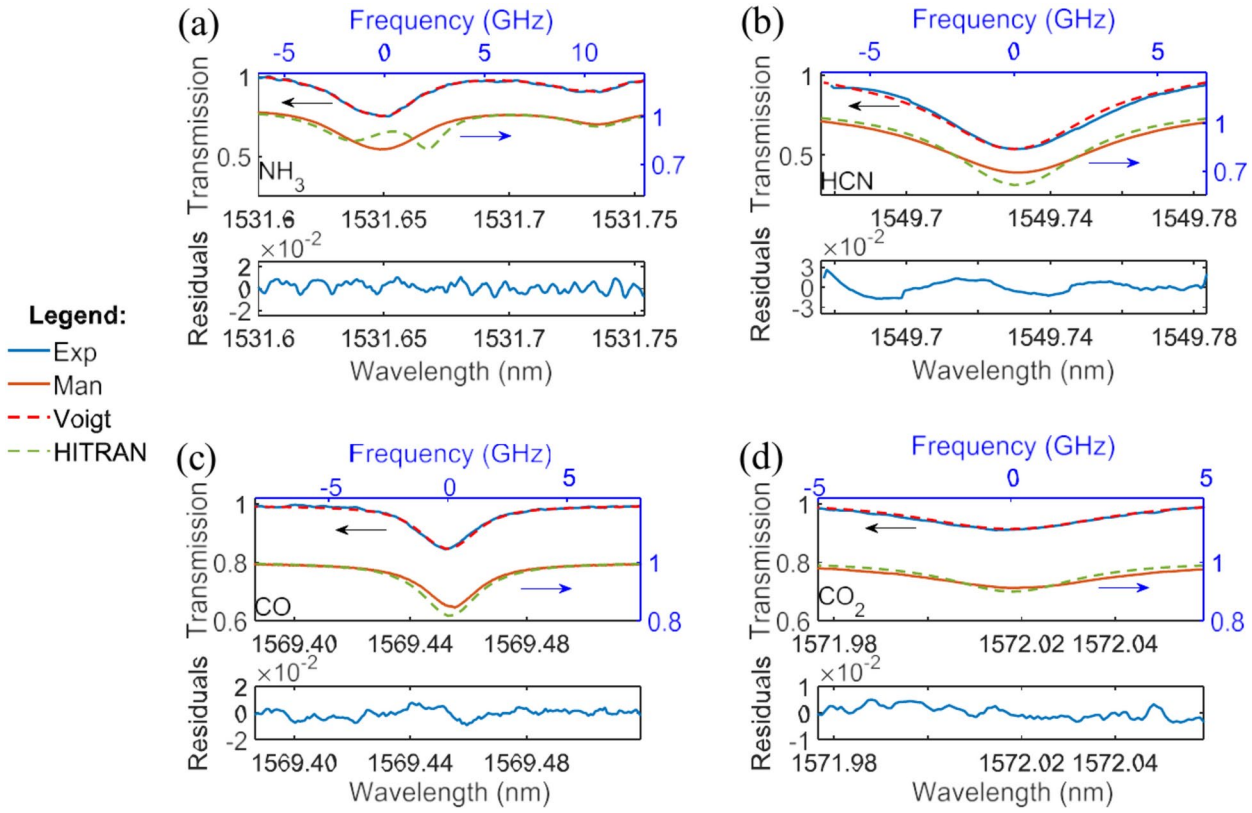

Fig. 5. Absorption lines of each gas: (**a**) NH_3 (@ 1531.67 nm), (**b**) HCN (@ 1549.73 nm), (**c**) CO (@ 1569.45 nm) and (**d**) CO_2 (@ 1572.02 nm), respectively. Experimental data (blue line) are fitted to a Voigt profile (red dashed line) and compared with the HITRAN database (green dashed line) and the manufacturer datasheet (referred to Man in legend and plotted with an orange line). The absorption lines have been centered at 0 GHz for clarity (upper x-axis). The residuals, corresponding to the Voigt function compared to the experimental data, are also plotted for each gas absorption.

Database parameters	Experimental		Voigt		HITRAN		Manufacturer	
	$\Delta\nu$ (GHz)	T	$\Delta\nu$ (GHz)	T	$\Delta\nu$ (GHz)	T	$\Delta\nu$ (GHz)	T
NH_3 @1531.67 nm	5.11	0.74	5.11	0.73	3.84	0.74	5.00	0.75
HCN @1549.73 nm	6.25	0.58	6.00	0.53	6.39	0.52	7.49	0.58
CO @1569.45 nm	2.44	0.84	2.44	0.84	3.66	0.85	2.35	0.84
CO_2 @1572.02 nm	4.86	0.91	4.86	0.90	4.86	0.90	6.07	0.91

Table 2. Comparison of the experimental spectral bandwidth ($\Delta\nu$) and transmittance (T) parameters of the four absorption profiles with the HITRAN and manufacturer databases. Experimental data are also fitted to a Voigt profile.

However, our experimental bandwidth and the one provided by the manufacturer are similar. Higher residual values from the absorption profile fitting are obtained for the HCN (about 0.03) compared to the other three gases. This can be explained by the lower CNR and Δf_{10} obtained for the corresponding OFC generated for this spectral region. Despite this, the resolution and sensitivity are found to be enough to measure the absorption lines for each gas under study, including a minimum absorbance of 0.43 dB, corresponding to the CO_2 absorption line. The entire acquisition time for the gas absorption measurements was less than 10 seconds for the set of the four gases, thereby demonstrating the stability of the dual-comb system with minimal error.

While our results demonstrate significant potential for commercial applications, several challenges must be addressed to realize full-scale deployment. These include further improving the robustness and long-term stability of the system, optimizing photonic integration for enhanced portability, and developing advanced calibration techniques to maintain measurement accuracy across diverse environmental conditions. Future research could focus on enhancing the tunability and spectral coverage of the dual-comb system by incorporating advanced laser designs with broader gain bandwidths. Moreover, exploring alternative modulation schemes and injection strategies might increase comb coherence and reduce residual errors further. Developing compact and fully integrated photonic platforms for dual-comb spectroscopy would also be a pivotal step toward practical, scalable solutions for a wide range of applications.

Conclusion

The emergence of optical systems capable of producing OFCs with numerous comb lines, adjustable channel spacing and wide spectral operation ranges, while ensuring low noise levels with maximum power efficiency, system simplicity, and cost-effectiveness, has garnered significant attention recently. In this work, we present an innovative multi-gas spectroscopy setup using a near-infrared dual-comb source with tunable operation range. The dual-comb framework comprises two gain- switched, low-repetition-rate optical frequency combs using FP lasers, externally injected by a tunable laser source. This system significantly reduces the complexity and costs associated with external excitation sources compared to conventional gain-switching laser systems while preserving OFC coherence[26]. Through meticulous selection of the FP mode for phase locking, along with careful consideration of line-spacing and optical span parameters, we demonstrate the generation of stable OFCs at different wavelengths. Our approach yields broad and flat spectra, boasting over 40 GHz bandwidth and a high number of tones (>400 lines) with a CNR of 24 dB at low repetition rates (100 MHz). Thus, highly coherent OFCs can be achieved by this laser scheme with an operation spectral range of more than 40 nm. Finally, we validate the utility of this system for gas-sensing applications. As a proof-of-concept demonstration, we analyze four different gas samples centered at 80 MHz RF spectral range. The experimental results demonstrate a good approximation to the HITRAN and manufacturer data, exhibiting a low residual value (0.3%). The simplicity and tunability inherent to our configuration open the door for potential photonic integration.

Methods

OFC generation

In order to generate the OFCs, two different stages are involved: the electrical and optical processes. In relation to the electrical stage, a combination of DC and AC signals are introduced in the laser for gain-switching operation. The signals are provided to the slave lasers through a bias tee with a bandwidth of 12.5 GHz, as shown in Fig. 6a. For this purpose, a laser diode controller (Arroyo ARO-4308) is used as the DC bias source for the slave laser (Laserscom, LDS-1550-FP-DIL-PM-FC/APC-0.5m). The free-running slave laser operates at 1550 nm, with a nominal modulation data rate of 2.5 Gbit/s and a threshold current of 11 mA. It is packaged in a 14-pin DIL socket, without a built-in optical isolator to allow OI. The gain switching operation is achieved by applying an amplified RF pulsed signal to the high-speed connector of the bias tee. These AC signals are usually generated by conventional excitation sources, such as high data-rate pulse pattern generators or arbitrary waveform generators. Nevertheless, these devices, despite their high resolution and stability properties, remain bulky and expensive. Therefore, we have used an approach to replace them with a low-cost alternative[26]. It comprises the use of a direct digital synthesizer (DDS) (Analog Devices AD9958) capable of producing two sine waves from a single, fixed-frequency reference clock. Two synchronized DDS channels operating at 500 Msa/s generate sinusoidal signals with slightly different repetition rates, with a tuning resolution of 0.12 Hz. In this case, a sinusoidal signal is initially used for driving SL1 with a peak-to-peak amplitude of 250 mV and a repetition rate of 100 MHz, while SL2 has a repetition rate of 100.01 MHz. For optimal pulse quality, an electrical preamplifier is also introduced. The amplified sinusoidal signal at 100 MHz is shown in Fig. 6b. However, as demonstrated in

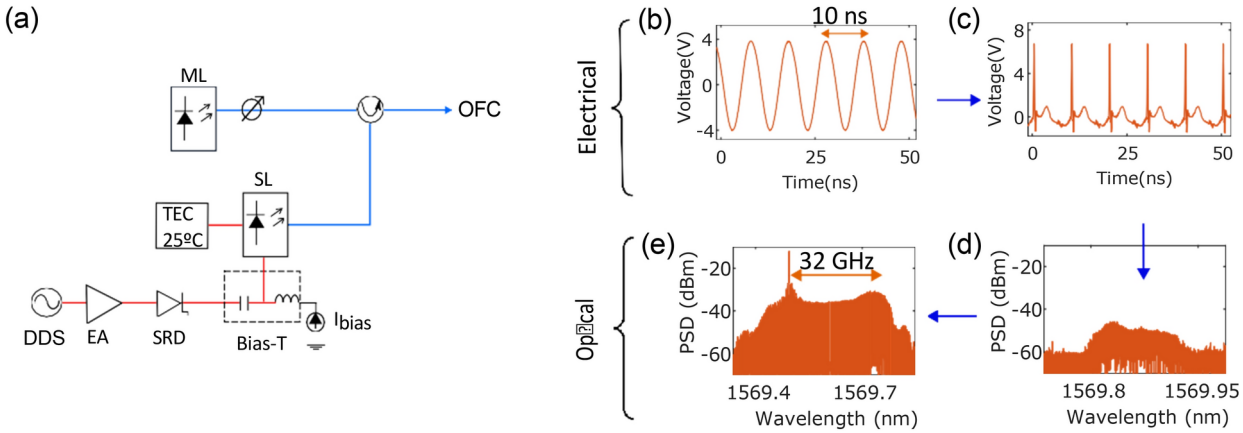

Fig. 6. (**a**) Schematic of the gain-switching OFC generation based on the use of a DC signal (bias current) and an RF signal supplied through a bias tee and frequency centered by a temperature controller (TEC). (**b**) The AC signal is based on an electrically-ampliflied (EA) sinusoidal signal generated from a Direct Digital Synthesizer (DDS). (**c**) The sine wave is then transformed into a pulsed signal by employing a Step-Recover Diode (SRD). (**d**) Optical spectrum of single longitudinal mode of a gain-switched FP laser after applying the corresponding AC and DC signals. (**e**) Optical spectrum of the gain-switched FP laser after inserting an external laser source for optical injection.

previous studies, the use of sinusoidal signals as the AC current is not sufficient to obtain broad and flat OFCs at low repetition rates (<500 MHz) with high-quality properties[13]. To overcome these limitations, pulsed signals are employed, facilitated by incorporating SRDs (Tekbox TBCG2), leading to pulsed signals with a sharp peak (7 V and 250 ps of pulse duration). These signals will be employed as the AC modulation for each laser. The temporal profile of this electrical signal is depicted in Fig. 6c.

Precise adjustment of the RF signal amplitude and the DC bias current is essential for the production of high-quality OFCs with optimal CNR. The resulting optical signal from the gain-switched FP laser is then analyzed using a high resolution (0.08 pm) BOSA, for spectral characterization. An example of the gain-switching operation of the FP laser with a bias current of 20 mA is presented in Fig. 6d. However, this method does not provide sufficiently high CNR and broad and flat spectra. To solve this, a tunable laser (Pure Photonics PPCL300) is incorporated in the optical setup for optical injection, providing an injection power that is adjusted to -3.5 dBm. The output OFC profile can be fine-tuned by carefully selecting the injection wavelength of the tunable ML. This optimization yields an expanded OFC bandwidth ($\backsim$ 40 GHz), with an increased number of tones (> 400 lines), as depicted in Fig. 6e when the laser is biased with 6 mA DC current. The tuning of the SL frequencies can be independently controlled by temperature controllers (see Fig. 6a). In this example, the SL is configured to a central wavelength of 1569.6 nm, while the injection wavelength of the ML is centered at 1569.5 nm. This wavelength shift of 15 GHz from the absorption line of interest is sufficient to mitigate instabilities around the injection wavelength that could potentially impact the accuracy of the absorption line measurement. The same meticulous procedure is applied to both slave lasers for the four spectral regions of interest. The production of the four flat-topped OFCs is accomplished through a careful selection of the injected power, central wavelength of the ML, bias current, and amplitude of the pulsed signal. We have not observed instabilities of the OFCs caused by fluctuations, rather than the stability being influenced by the dynamics of the FP lasers and the injection conditions. Operating at 100 MHz balances the need for adequate comb line spacing to resolve gas absorption features with practical system constraints, such as detector bandwidth and comb line power. While higher repetition rates can offer benefits like faster measurements, they also introduce challenges, including reduced detection sensitivity and the need for higher-bandwidth electronics, requiring careful trade-offs[13–15].

Down-converted DCS

To analyze the experimental data, we developed a custom MATLAB® software. Figure 7 illustrates a block diagram of the main steps followed for data processing. The experimental data comprise two sets of temporal interferograms, one from the reference arm and the other containing gas-related information, both recorded by the oscilloscope. These datasets consist of $8{\cdot}10^5$ points (acquired at 313 MSa/s within a 2.5 ms time window), and are repeated 500 times for averaging purposes. The experimental data is then Fourier transformed using the Fast Fourier Transform (FFT) function, translating the information into the spectral domain. Subsequently, the 500 spectra are averaged to mitigate the background noise during the measurement.

Afterward, a specific spectral region encompassing the absorption line of interest is defined. This process involves the following steps: (i) Initially, the program identifies the minimum of the envelope associated with the gas-related information. This value corresponds to the absorption depth of the gas under test. (ii) Subsequently, the code locates the mean intensity value of the reference dataset, representing the maximum intensity of the gas-related trace. It is noteworthy that due to the insertion losses (> 2.5 dB) introduced by each gas cell, the gas measurement has less CNR than the reference. (iii) Finally, the spectral window is defined by identifying the

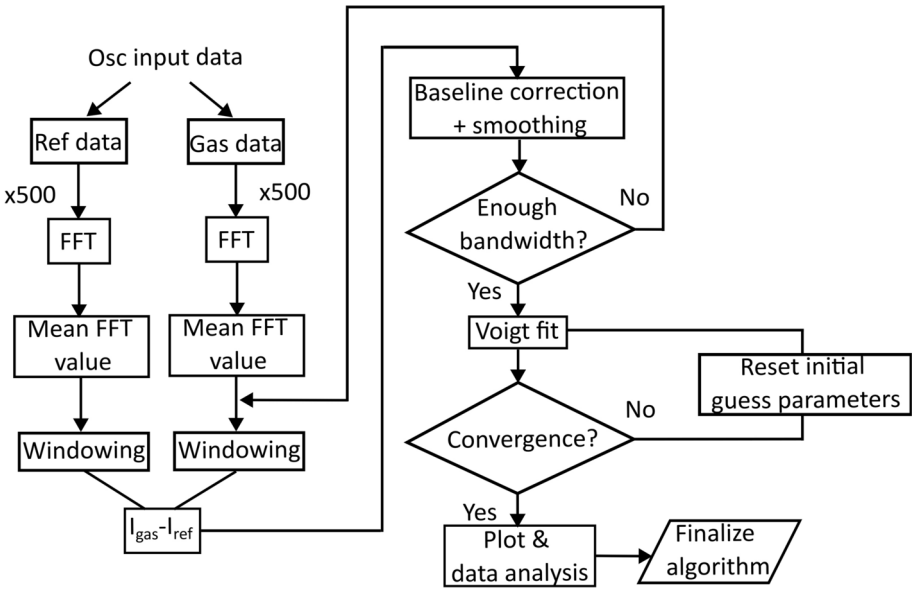

Fig. 7. Main flow of the code for the acquisition of the absorption profile.

first intensity value of the gas trace that coincides with the reference one. Therefore, a cropped RF spectrum is obtained. This effect will be referred in this work as windowing. This ensures that more than 150 optical tones fall within this spectral region, corresponding to a bandwidth of 20 MHz in the RF domain. It is important to note that a 20 GHz bandwidth in the spectral domain translates to a 20 MHz window in the RF spectrum after applying the compression factor, as defined in the dual-comb spectroscopy section.

Once the spectral window is defined, the program retrieves the maximum intensity values of the tones from both cropped RF spectra. This process generates two datasets, one comprising intensity values of the reference arm as a function of wavelength, and the other containing gas-related information. Subsequently, the gas absorption is derived by subtracting the intensity values obtained in the reference arm from those of the gas cell ($I_{gas} - I_{ref}$). This experimental absorption can be optimized by applying a linear baseline correction to the transmission curve. Additionally, a smoothing function is employed to reduce random noises in the measurement. Subsequently, the code assesses whether the previously defined spectral window encompasses a sufficiently broad bandwidth to capture a well-defined absorption of the gas under test. This ensures that the spectral window surpasses the width of the absorption line. In this case, a window width of 20 MHz is selected for all the measurements.

Finally, the resulting data are normalized and fitted to a Voigt function to compare these results with the HITRAN[39] and manufacturer data. The convergence of this fit is evaluated by minimizing their differences (standard deviation). Otherwise, the code is reset by varying the initial guess parameters (absorption depth, bandwidth, etc.). The experimental transmission curves are presented on a linear scale for comparison purposes, as shown in Fig. 5. Moreover, the residuals of this Voigt fit in relation to the experimental values are also included in this representation.

Data availability

The datasets used and/or analysed during the current study available from the corresponding author on reasonable request.

Received: 25 November 2024; Accepted: 10 February 2025
Published online: 04 March 2025

References

1. Picqué, N. & Hänsch, T. Frequency comb spectroscopy. *Nat. Photon.* **13**, 146–157 (2019).
2. Imran, M., Anandarajah, P., Kaszubowska-Anandarajah, A., Sambo, N. & Potí, L. A survey of optical carrier generation techniques for terabit capacity elastic optical networks. *IEEE Commun. Surv. Tutor.* **20**, 211–263 (2018).
3. Poli, N., Oates, C., Gill, P. & Tino, G. Optical atomic clocks. *La Rivista del Nuovo Cimento* **36**, 555–624 (2013).
4. Coddington, I., Swann, W. C., Nenadovic, L. & Newbury, N. R. Rapid and precise absolute distance measurements at long range. *Nat. Photon.* **3**, 351–356 (2009).
5. van den Berg, S. A., van Eldik, S. & Bhattacharya, N. Mode-resolved frequency comb interferometry for high-accuracy long distance measurement. *Sci. Rep.* **5**, 14661 (2015).
6. Haus, H. A. Mode-locking of lasers. *IEEE J. Sel. Top. Quantum Electron.* **6**, 1173–1185 (2000).
7. Pasquazi, A. et al. Micro-combs: A novel generation of optical sources. *Phys. Reports* **729**, 1–81 (2018).
8. Parriaux, A., Hammani, K. & Millot, G. Electro-optic frequency combs. *Adv. Opt. Photon.* **12**, 223–287 (2020).
9. Dúill, S. P., Zhou, R., Anandarajah, P. M. & Barry, L. P. Analytical approach to assess the impact of pulse-to-pulse phase coherence of optical frequency combs. *IEEE J. Quantum Electron.* **51**, 1–8 (2015).

10. Rosado, A. et al. Experimental study of optical frequency comb generation in gain-switched semiconductor lasers. *Opt. Laser Technol.* **108**, 542–550 (2018).
11. Anandarajah, P. M. et al. Generation of coherent multicarrier signals by gain switching of discrete mode lasers. *IEEE Photonics J.* **3**, 112–122 (2011).
12. Anandarajah, P. M., Dúill, S. P. Ó., Zhou, R. & Barry, L. P. Enhanced optical comb generation by gain-switching a single-mode semiconductor laser close to its relaxation oscillation frequency. *IEEE J. Sel. Top. Quantum Electron.* **21**, 592–600 (2015).
13. Rosado, A. et al. Numerical and experimental analysis of optical frequency comb generation in gain-switched semiconductor lasers. *IEEE J. Quantum Electron.* **55**, 1–12 (2019).
14. Quirce, A. et al. Nonlinear dynamics induced by optical injection in optical frequency combs generated by gain-switching of laser diodes. *IEEE Photonics J.* **12**, 1–14 (2020).
15. Rosado, A. et al. Enhanced optical frequency comb generation by pulsed gain-switching of optically injected semiconductor lasers. *Opt. Express* **27**, 9155–9163 (2019).
16. Quirce, A., Kelleher, B. & Valle, A. Optical injection locking of longitudinal modes in a discrete mode laser: Application in gain-switched optical frequency combs. *J. Light. Technol.* **42**, 3799–3806 (2024).
17. Gutierrez Pascual, M. D. et al. Inp photonic integrated externally injected gain switched optical frequency comb. *Opt. Lett.* **42**, 555–558 (2017).
18. López-Querol, P., Quevedo-Galán, C., Pérez-Serrano, A., Tijero, J. M. G. & Esquivias, I. Low repetition rate optical frequency combs generated by pulsed gain-switching of semiconductor lasers. In *2021 27th International Semiconductor Laser Conference (ISLC)*, 1–2 (IEEE, 2021).
19. Rosado, A. et al. Optical frequency comb generation via pulsed gain-switching in externally-injected semiconductor lasers using step-recovery diodes. *Opt. Laser Technol.* **131**, 106392 (2020).
20. Quevedo-Galán, C., Pérez-Serrano, A., López-Delgado, I. E., Tijero, J. M. G. & Esquivias, I. Dual-comb spectrometer based on gain-switched semiconductor lasers and a low-cost software-defined radio. *IEEE Access* **9**, 92367–92373 (2021).
21. Coddington, I., Newbury, N. & Swann, W. Dual-comb spectroscopy. *Optica* **3**, 414–426 (2016).
22. Sugiyama, Y., Kashimura, T., Kashimoto, K., Akamatsu, D. & Hong, F. Precision dual-comb spectroscopy using wavelength-converted frequency combs with low repetition rates. *Sci. Rep.* **13**, 2549 (2023).
23. Hoghooghi, N. et al. Broadband coherent cavity-enhanced dual-comb spectroscopy. *Optica* **6**, 28–33 (2019).
24. Kawai, A., Kageyama, T., Horisaki, R. & Ideguchi, T. Compressive dual-comb spectroscopy. *Sci. Rep.* **11**, 13494 (2021).
25. Quevedo-Galán, C. et al. Gain-switched semiconductor lasers with pulsed excitation and optical injection for dual-comb spectroscopy. *Opt. Express* **28**, 33307–33317 (2020).
26. Monroy, L., Pérez-Serrano, A., Tijero, J. M. G. & Esquivias, I. Low-cost dual-comb spectrometer for CO2 monitoring based on gain-switched semiconductor lasers. *Results Phys.* **58**, 107516 (2024).
27. Rosado, A., Fernández-Ruiz, M. R., Corredera, P., Tijero, J. M. G. & Esquivías, I. High-density and broad band optical frequency combs generated by pseudo-random phase modulation of optically injected gain-switched semiconductor lasers. *Opt. Laser Technol.* **163**, 109312 (2023).
28. Quevedo-Galán, C., Rosado, A., Pérez-Serrano, A., Tijero, J. M. G. & Esquivias, I. Dual-comb spectroscopy with enhanced resolution by pseudorandom phase modulation of gain-switched optical pulses. *J. Light. Technol.* **2**, 109312 (2024).
29. Prior, E. et al. Expansion of vcsel-based optical frequency combs in the sub-thz span: Comparison of non-linear techniques. *J. Light. Technol.* **34**, 4135–4142 (2016).
30. Lakshmijayasimha, P. D., Kaszubowska-Anandarajah, A., Martin, E. P., Landais, P. & Anandarajah, P. M. Expansion and phase correlation of a wavelength tunable gain-switched optical frequency comb. *Opt. Express* **27**, 16560–16570 (2019).
31. Lakshmijayasimha, P. D., Anandarajah, P. M., Landais, P. & Kaszubowska-Anandarajah, A. Optical frequency comb expansion using mutually injection-locked gain-switched lasers. *Appl. Sci.* **11**, 7108 (2021).
32. Deseada Gutierrez Pascual, M. *et al.* Cascaded fabry-pérot lasers for coherent expansion of wavelength tunable gain switched comb. In *2014 The European Conference on Optical Communication (ECOC)*, 1–3 (IEEE, 2014).
33. Deseada Gutierrez Pascual, M. *et al.* Dual mode injection locking of a fabry-pérot laser for tunable broadband gain switched comb generation. In *2015 European Conference on Optical Communication (ECOC)*, 1–3, https://doi.org/10.1109/ECOC. 2015.7341716 (2015).
34. Lakshmijayasimha, P. D., Kaszubowska-Anandarajah, A., Srivastava, M., Martin, E. P. & Anandarajah, P. M. Generation of a wideband OFC by the correlation of multiple modes of a gain-switched fabry pérot laser. *J. Light. Technol.* (2023).
35. Zhou, R. et al. 40nm wavelength tunable gain-switched optical comb source. *Opt. Express* **19**, B415–B420 (2011).
36. Jain, G., Gutierrez-Pascual, D., Wallace, M. J., Donegan, J. F. & Anandarajah, P. M. Experimental investigation of external optical injection and its application in gain-switched wavelength tunable optical frequency comb generation. *J. Light. Technol.* **39**, 5884–5895 (2021).
37. Martin, E. P. et al. Stability characterisation and application of mutually injection locked gain switched optical frequency combs for dual comb spectroscopy. *J. Light. Technol.* **41**, 4516–4521 (2023).
38. Long, D. A. et al. Multiheterodyne spectroscopy with optical frequency combs generated from a continuous-wave laser. *Opt. Lett.* **39**, 2688–2690 (2014).
39. Molecular line-by-line search. HITRAN database. Accessed 29 Nov 2023. hitran.org/lbl/5?output_format_id=1&iso_ids_list=7&vib_bands=&numin=5555&numax=6666.

Acknowledgements

The authors want to thank A. Rosado and C. Quevedo-Galán for their fruitful comments. This work was supported by grant TED2021-131957B-100 funded by MCIN/ AEI /https://doi.org/10.13039/501100011033 and by the European Union NextGenerationEU/PRTR, and grant PID2021-1234590B-C21 funded by MCIN/ AEI /https://doi.org/10.13039/501100011033 and ERDF "A way of making Europe".

Author contributions

L. Monroy: Writing-original draft, Investigation, Conceptualization. A. Pérez-Serrano: Funding acquisition, Conceptualization, Writing—review & editing. J. M. G. Tijero: Funding acquisition, Supervision, Writing—review & editing. I. Esquivias: Funding acquisition, Conceptualization, Supervision, Writing—review & editing.

Declarations

Competing interests

The authors declare no competing interests.

Additional information

Correspondence and requests for materials should be addressed to L.M. or J.M.G.T.

Reprints and permissions information is available at www.nature.com/reprints.

Publisher's note Springer Nature remains neutral with regard to jurisdictional claims in published maps and institutional affiliations.

Open Access This article is licensed under a Creative Commons Attribution-NonCommercial-NoDerivatives 4.0 International License, which permits any non-commercial use, sharing, distribution and reproduction in any medium or format, as long as you give appropriate credit to the original author(s) and the source, provide a link to the Creative Commons licence, and indicate if you modified the licensed material. You do not have permission under this licence to share adapted material derived from this article or parts of it. The images or other third party material in this article are included in the article's Creative Commons licence, unless indicated otherwise in a credit line to the material. If material is not included in the article's Creative Commons licence and your intended use is not permitted by statutory regulation or exceeds the permitted use, you will need to obtain permission directly from the copyright holder. To view a copy of this licence, visit http://creativecommons.org/licenses/by-nc-nd/4.0/.

© The Author(s) 2025